Available online at www.sciencedirect.com
SCIENCE DIRECT®
Pattern Recognition Letters 26 (2005) 2006–2014
Pattern Recognition Letters
www.elsevier.com/locate/patrec

Color transfer based remote sensing image fusion using non-separable wavelet frame transform

Zhenhua Li [a,*], Zhongliang Jing [a,b], Xuhong Yang [a], Shaoyuan Sun [a]

[a] *Institute of Aerospace Information and Control, School of Electronic, Information and Electrical Engineering, Shanghai Jiaotong University, Shanghai 200030, PR China*
[b] *Institute of Aerospace Science and Technology, Shanghai Jiaotong University, Shanghai 200030, PR China*

Received 11 April 2004; received in revised form 18 February 2005
Available online 29 April 2005

Communicated by M.A.T. Figueiredo

Abstract

In order to fuse two registered high spatial resolution panchromatic image and low spatial resolution multispectral image of the same scene, we proposed a new color transfer based fusion algorithm by using the non-separable wavelet frame transform (NWFT). Three bands are selected from the source multispectral image as the channels to be fused. A grayscale image is obtained by averaging these three bands. Histogram matching is performed on the source panchromatic image to obtain a new panchromatic image with a uniform histogram as the grayscale image acquired from the source multispectral image. The histogram matched panchromatic image is decomposed by the NWFT. The lowest frequency subband of the NWFT coefficients is substituted by the grayscale image acquired from the source multispectral image in order to produce the composite NWFT coefficients. A composite image is obtained by performing the inverse NWFT transform on the combined coefficients. Three bands selected from the source multispectral image are mapped into the RGB (red–green–blue) color space. The color information (strictly speaking, it is the spectral information of the source multispectral image) is transferred into the composite image by using a color transfer method in order to get the finally fused image. Experiment results show that the proposed algorithm works well in remote sensing image fusion.

Keywords: Remote sensing; Image fusion; Color transfer; Non-separable wavelet frame transform

1. Introduction

With the rapid improvement of sensor technology, multisensor data, which often contain complementary and redundant information about the

* Corresponding author. Tel./fax: +86 021 6293 2120.
E-mail address: randy_lee@sjtu.edu.cn (Z. Li).

0167-8655/$ - see front matter © 2005 Elsevier B.V. All rights reserved.
doi:10.1016/j.patrec.2005.02.010

region surveyed, are now obtained for remote sensing. Fusion of multisensor data becomes a promising research area. Through combining registered images generated by different imaging systems, image fusion can produce new images with more complete information that are more suitable for human vision perception, object detection and automatic target recognition. Image fusion can be divided into signal, pixel, feature, and symbol levels. This paper mainly considers pixel level image fusion. Multispectral imaging sensors collect poor spatial resolution multispectral images, while panchromatic imaging sensors provide adequate spatial resolution panchromatic images. In remote sensing, fusing high spatial resolution panchromatic images with low spatial resolution multispectral images becomes popular since it can produce high spatial resolution multispectral images.

Various remote sensing image fusion algorithms have been proposed. The commonly used remote sensing image fusion algorithms include those based on the IHS transform (Carper et al., 1990; Chavez et al., 1991), the principal component analysis (PCA) (Chavez and Kwarteng, 1989; Chavez et al., 1991), the Brovey transform (Civco et al., 1995), and the high-pass filtering (Shettigara, 1992). Recently, multiresolution decomposition based algorithms are widely used in remote sensing image fusion, such as the DWT based fusion algorithms (Li et al., 1995; Yockey, 1995; Zhou et al., 1998) and the DWFT based fusion algorithm (Li et al., 2002). Both the DWT and the DWFT can decompose a signal into several components, each of which captures information present at a given scale. The DWT or the DWFT decomposition of an image can break down into 1-dimensional wavelet decomposition on rows and columns respectively. In practice, for 2-dimensional signal $f(x,y) \in L^2(R^2)$, it cannot be processed separately in x and y directions in most cases. The 2-dimensional separable wavelet transform also yields a shift variant data representation by the downsampling process and is not appropriate for multisensor image fusion. The non-separable wavelet transform (Kovačević and Vetterli, 1992, 1995) allows true processing of images. Images are treated as areas instead of rows and columns. The advantage of the non-separable wavelet transform is having better frequency characteristics, directional properties and more degree of freedom, resulting in better design. By eliminating the decimator and interpolator process and changing the filter coefficients of the non-separable wavelet transform, we will obtain the non-separable wavelet frame transform (Pan and Wang, 1999). All the subbands after the NWFT decomposition will have the same size as the source image. The NWFT has the property of shift-invariance and is more suitable for image fusion. In this paper, we developed an approach based on the NWFT for the fusing of multispectral and panchromatic remote sensing images.

This paper is organized as follows. The general image fusion methods in remote sensing are described in Section 2. In Section 3, the proposed color transfer based image fusion algorithm using the NWFT is presented in details. Section 4 shows the experimental results and comparison with conventional methods. Section 5 concludes the paper.

2. General image fusion methods in remote sensing

2.1. Fusion with the intensity-hue-saturation (IHS) transform

The IHS transform (Carper et al., 1990; Chavez et al., 1991) is one of the widespread image fusion methods in the remote sensing community. Three bands of the source multispectral image are mapped into the RGB color space and the RGB color space is then transformed to the IHS color space:

$$\begin{bmatrix} I \\ V_1 \\ V_2 \end{bmatrix} = \begin{bmatrix} \frac{1}{3} & \frac{1}{3} & \frac{1}{3} \\ -\frac{\sqrt{2}}{6} & -\frac{\sqrt{2}}{6} & \frac{2\sqrt{2}}{6} \\ \frac{1}{\sqrt{2}} & -\frac{1}{\sqrt{2}} & 0 \end{bmatrix} \begin{bmatrix} R \\ G \\ B \end{bmatrix}, \tag{1}$$

$$H = \tan^{-1}\left(\frac{V_2}{V_1}\right), \tag{2}$$

$$S = \sqrt{V_1^2 + V_2^2}, \tag{3}$$

where I is the intensity component, H is the hue component, S is the saturation component, V_1 and V_2 are the intermediate variables. Fusion is performed by replacing I with the source panchromatic image. Finally, the fused image is obtained by performing the inverse IHS transform. The IHS transform based image fusion algorithm can preserve the same spatial resolution as the source panchromatic image but seriously distort the spectral (color) information in the source multispectral image.

2.2. Fusion with the discrete wavelet transform (DWT)

Zhou et al. (1998) developed a DWT based fusion algorithm to merge Landsat TM (Thematic Mapper) multispectral and SPOT (System Pour l'Observation de la Terre) panchromatic images. The source SPOT panchromatic image and each spectral band of the source TM multispectral image are decomposed into an orthogonal wavelet representation at a given coarser resolution, which consisted of a low frequency approximation image and a set of high frequency images. Band-by-band, the fused images were derived by performing the inverse DWT using the approximation image from each band of the source TM multispectral image and detail images from the source SPOT panchromatic image. The performance of this fusion algorithm is better than those based on the IHS transform, the principal component analysis (PCA), and the Brovey transform.

2.3. Fusion with the discrete wavelet frame transform (DWFT)

Li et al. (2002) developed a DWFT based fusion algorithm for Landsat TM multispectral and SPOT panchromatic image fusion. The source images are first decomposed using the DWFT. Wavelet coefficients from the lowest frequency subband of each spectral band of the source TM multispectral image and the high frequency subbands of the source SPOT panchromatic image are combined, and the fused image is then reconstructed by performing the inverse DWFT. The performance of the DWFT based algorithm outperforms the DWT based fusion algorithms (Li et al., 1995; Yockey, 1995; Zhou et al., 1998).

3. Color transfer based fusion algorithm using the non-separable wavelet frame transform (NWFT)

3.1. Color transfer

Ruderman et al. developed a new color space called $l\alpha\beta$ (Ruderman et al., 1998). This space is based on the data-driven human perception research that assumes the human visual system is ideally suited for processing natural scenes. There is little correlation between the axes in $l\alpha\beta$ space. We can apply different operations in different channels with some confidence that undesirable cross-channel artifacts will not occur. Reinhard et al. (2001) used this $l\alpha\beta$ color space to transfer colors between two color images. Colors from a source color image are transferred to a second color image using a simple but surprisingly successful procedure. Welsh et al. (2002) introduced a general technique for "coloring" grayscale images by transferring colors between a source color image and a target grayscale image. When converting the RGB color space to the $l\alpha\beta$ color space, the RGB color space is changed into the LMS cone space:

$$\begin{bmatrix} L \\ M \\ S \end{bmatrix} = \begin{bmatrix} 0.3811 & 0.5783 & 0.0402 \\ 0.1967 & 0.7244 & 0.0782 \\ 0.0241 & 0.1288 & 0.8444 \end{bmatrix} \begin{bmatrix} R \\ G \\ B \end{bmatrix}. \quad (4)$$

The data in this color space shows a great deal of skew, which can be largely eliminated by converting the data to the logarithmic space:

$$\Gamma = \log L, \quad (5)$$

$$\Omega = \log M, \quad (6)$$

$$\Psi = \log S. \quad (7)$$

In order to decorrealate these axes, the logarithmic color space is further transformed to get three orthogonal axes:

$$\begin{bmatrix} l \\ \alpha \\ \beta \end{bmatrix} = \begin{bmatrix} \frac{1}{\sqrt{3}} & 0 & 0 \\ 0 & \frac{1}{\sqrt{6}} & 0 \\ 0 & 0 & \frac{1}{\sqrt{2}} \end{bmatrix} \begin{bmatrix} 1 & 1 & 1 \\ 1 & 1 & -2 \\ 1 & -1 & 0 \end{bmatrix} \begin{bmatrix} \Gamma \\ \Omega \\ \Psi \end{bmatrix}. \tag{8}$$

In this color space, l axis represents an achromatic channel, while the α and β axes are chromatic yellow–blue and red–green opponent channels. According to Ruderman et al. (1998), the data in this space are symmetrical and compact.

We can convert from the $l\alpha\beta$ color space to the RGB color space by the following inverse operations:

$$\begin{bmatrix} \Gamma \\ \Omega \\ \Psi \end{bmatrix} = \begin{bmatrix} 1 & 1 & 1 \\ 1 & 1 & -1 \\ 1 & -2 & 0 \end{bmatrix} \begin{bmatrix} \frac{1}{\sqrt{3}} & 0 & 0 \\ 0 & \frac{1}{\sqrt{6}} & 0 \\ 0 & 0 & \frac{1}{\sqrt{2}} \end{bmatrix} \begin{bmatrix} l \\ \alpha \\ \beta \end{bmatrix} \tag{9}$$

and

$$\begin{bmatrix} R \\ G \\ B \end{bmatrix} = \begin{bmatrix} 4.4679 & -3.5873 & 0.1193 \\ -1.2186 & 2.3809 & -0.1624 \\ 0.0497 & -0.2439 & 1.2045 \end{bmatrix} \begin{bmatrix} 10^{\Gamma} \\ 10^{\Omega} \\ 10^{\Psi} \end{bmatrix}. \tag{10}$$

Colors can be transferred from the source color image to the target grayscale image by combining the chromaticity values (α and β) and the intensities of the grayscale image.

3.2. The 2-dimensional NWFT

The 2-dimensional non-separable wavelet transform (Kovačević and Vetterli, 1992, 1995) is similar to the 1-dimensional case. The low-pass component of an image is repeatedly filtered and sub-sampled resulting in another low-pass image and another detail image. However, sub-sampling is not performed by retaining every second column and row, as it is in the separable case, but performed on a non-separable sampling matrix. There are many kinds of sampling matrixes. The sampling matrix used in this paper is given by

$$\boldsymbol{D} = \begin{bmatrix} 1 & 1 \\ 1 & -1 \end{bmatrix}. \tag{11}$$

The down-sampling process of an image f using the sampling matrix $\boldsymbol{D}$ is defined as

$$f_{\downarrow \boldsymbol{D}}(\boldsymbol{K}) = f(\boldsymbol{D} \cdot \boldsymbol{K}), \quad \boldsymbol{K} \in \boldsymbol{Z}^2, \tag{12}$$

where $\boldsymbol{Z}$ is the set of integer, $\boldsymbol{K}$ is the pixel coordinate, $f(\cdot)$ is the pixel intensity of image f.

The up-sampling process of an image f using the sampling matrix $\boldsymbol{D}$ is defined as

$$f_{\uparrow \boldsymbol{D}}(\boldsymbol{K}) = \begin{cases} f(\boldsymbol{D}^{-1} \cdot \boldsymbol{K}), & \text{if } \boldsymbol{K} = \boldsymbol{D} \cdot \boldsymbol{I} \text{ and } \boldsymbol{I} \in \boldsymbol{Z}^2, \\ 0, & \text{otherwise.} \end{cases} \tag{13}$$

By eliminating the resampling process and changing the filter coefficients of the non-separable wavelet transform, we will obtain the non-separable wavelet frame transform (Pan and Wang, 1999). The analysis and synthesis structure of the 2-dimensional NWFT is shown in Fig. 1. The NWFT coefficients of an image f are calculated as

$$\begin{cases} g_{i+1}(\boldsymbol{K}) = [G_0]_{\uparrow \boldsymbol{D}^i} * f_i(\boldsymbol{K}), \\ f_{i+1}(\boldsymbol{K}) = [H_0]_{\uparrow \boldsymbol{D}^i} * f_i(\boldsymbol{K}), \end{cases} \quad i = 0, 1, \ldots, N-1, \tag{14}$$

where H_0 and G_0 are the 2-dimensional analysis prototype filters, $[H_0]_{\uparrow \boldsymbol{D}^i}$ and $[G_0]_{\uparrow \boldsymbol{D}^i}$ are the dilated version of low-pass filter H_0 and high-pass filter G_0, $f_0(\boldsymbol{K}) = f(\boldsymbol{K})$, N is the decomposition level. In Fig. 1, H_1 and G_1 are the 2-dimensional synthesis prototype filters.

The design of 2-dimensional non-separable filters is generally more difficult than the design of

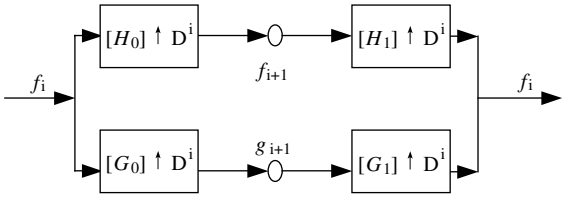

Fig. 1. The analysis and synthesis structure of the 2-dimensional NWFT.

1-dimensional filters. McClellan transformation (Kovačević and Vetterli, 1992) has been shown to be a useful technique for designing 2-dimensional non-separable filters. The method can transform 1-dimensional prototype filters into 2-dimensional zero phase FIR filters, and the 2-dimensional filters parameterized by the McClellan transformation have the properties of the 1-dimensional prototype filters.

Let $\{h(m)\,|\,m = 1,2,\ldots,M\}$ be the impulse response of symmetric zero phase filter ($h(m) = h(-m)$). The Fourier transform of this zero phase symmetric filter can be written as a function of $\cos(m\varpi)$:

$$\widehat{H}(\varpi) = \sum_{m=0}^{M} a(m)\cos(m\varpi), \tag{15}$$

where $a(0) = h(0)$ and $a(m) = 2h(m)$, $m \neq 0$, $(2M + 1)$ is the length of the 1-dimensional filter. Using Tchebycheff polynomials, $\cos(m\varpi)$ can be replaced by $T_m[\cos(\varpi)]$, where $T_m[\cdot]$ is the mth Tchebycheff polynomial, and thus $\widehat{H}(\varpi)$ can be rewritten as a polynomial of $\cos(\varpi)$:

$$\widehat{H}(\varpi) = \sum_{m=0}^{M} a(m)T_m[\cos(\varpi)]. \tag{16}$$

The idea of the McClellan transformation is to replace $\cos(\varpi)$ by a zero phase 2-dimensional filter $\widehat{F}(\varpi_1,\varpi_2)$, hence resulting in an overall zero phase 2-dimensional filter:

$$\widehat{H}(\varpi_1,\varpi_2) = \sum_{m=0}^{M} a(m)T_m\left[\widehat{F}(\varpi_1,\varpi_2)\right]. \tag{17}$$

In the context of filter banks, this transformation can only be applied to the biorthogonal case for the requirement of zero phase response. Typically $\widehat{F}(\varpi_1,\varpi_2)$ is chosen as

$$\widehat{F}(\varpi_1,\varpi_2) = \tfrac{1}{2}[\cos(\varpi_1) + \cos(\varpi_2)]. \tag{18}$$

The NWFT has two advantages: less constraint on filters and shift invariance. After N level decomposition of an image $f(x,y)$, we will get several high-pass subbands coefficients $\{g_i(x,y)\,|\,i = 1,2,\ldots,N\}$ and one low-pass subband $f_N(x,y)$, where $(x,y) \in Z^2$ are the coordinates of image pixels. Each frequency subband has the same size as the source image.

3.3. The proposed remote sensing image fusion algorithm

In this paper, we proposed a novel color transfer based remote sensing image fusion algorithm using the NWFT. The block diagram of our algorithm is shown in Fig. 2. Before image fusion, the source multispectral image and the source panchromatic image should be registered. When being registered to the high spatial resolution panchromatic image, the low spatial resolution multispectral image needs to be resampled. We suppose the registration process has been performed before image fusion. There are eight steps in our fusion algorithm.

Step 1. Three bands are selected from the source multispectral bands say (B_1, B_2, B_3, B_4, etc.). The three bands to be fused can also be obtained by combining the source multispectral bands, for example:

$$\text{Band } A = \frac{B_5 + B_7}{2},\quad \text{Band } B = \frac{B_3 + B_4}{2},\quad \text{and}\quad \text{Band } C = \frac{B_1 + B_2}{2}. \tag{19}$$

Step 2. The three bands selected from the source multispectral image are averaged to get a grayscale image:

$$I_{\text{ave}} = \frac{\text{Band } A + \text{Band } B + \text{Band } C}{3}. \tag{20}$$

Step 3. Performing histogram matching on the source panchromatic image to obtain a new panchromatic image I_{PAN} with a uniform histogram as I_{ave}. Histogram matching is the process of modifying the histogram of an image to best match the histogram of another image.

Step 4. The NWFT decomposition is performed on the histogram matched image I_{PAN}. For N level decomposition, we will get

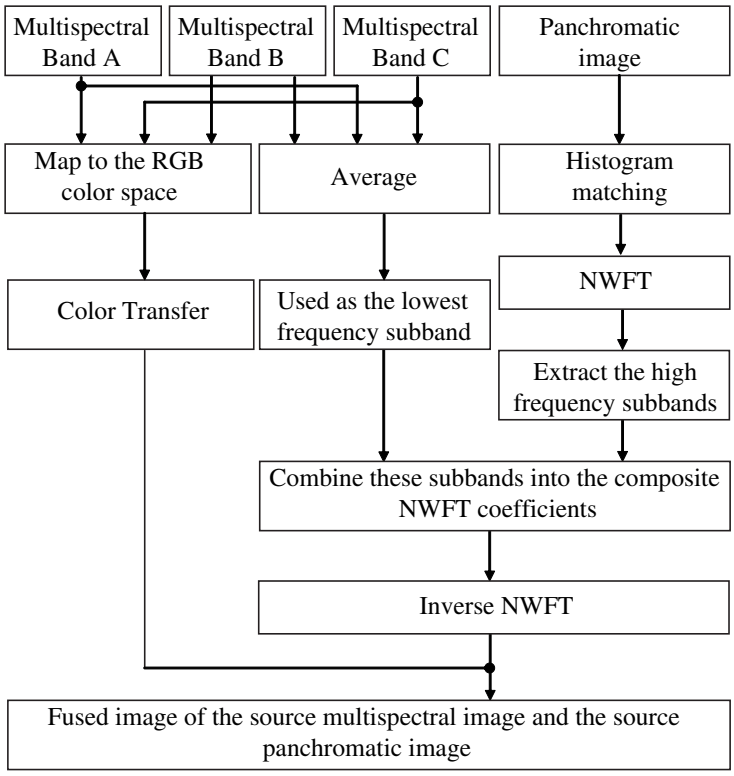

Fig. 2. The block diagram of the proposed image fusion algorithm.

$N+1$ subbands: high frequency subbands g_i^{PAN}, $(i = 1, 2, \ldots, N)$, and the lowest frequency subband f_N^{PAN}.

Step 5. The composite NWFT coefficients are calculated as

$$f_N^T = I_{\mathrm{ave}}, \tag{21}$$

$$g_i^T = g_i^{\mathrm{PAN}}, \quad i = 1, 2, \ldots, N. \tag{22}$$

Step 6. A composite image I_T is obtained by performing the inverse NWFT on the combined coefficients.

Step 7. Three bands selected from the source multispectral image are mapped into the RGB color space:

$$L_R = \mathrm{Band}\ A, \quad L_G = \mathrm{Band}\ B, \quad L_B = \mathrm{Band}\ C. \tag{23}$$

Then the RGB color space is converted into the $l\alpha\beta$ color space: l_S, α_S, β_S. Color transfer is performed between the color image and the composite image I_T. The achromatic channel of I_T is calculated as

$$l_T = \sqrt{3}\log I_T. \tag{24}$$

In the process of color transfer, the chromaticity values (α_S and β_S) are preserved, but the achromatic channel l_S is substituted by l_T. In order to eliminate the influence of overall illumination level changes between the color image and the composite image, we substitute l_S by

$$l' = (l_T - \langle l_T \rangle) \cdot \frac{\sigma_S^l}{\sigma_T^l} + \langle l_S \rangle, \tag{25}$$

where $\langle l_S \rangle$ and $\langle l_T \rangle$ are the means of l_S and l_T, respectively, σ_S^l and σ_T^l are the standard deviations of l_S and l_T, respectively.

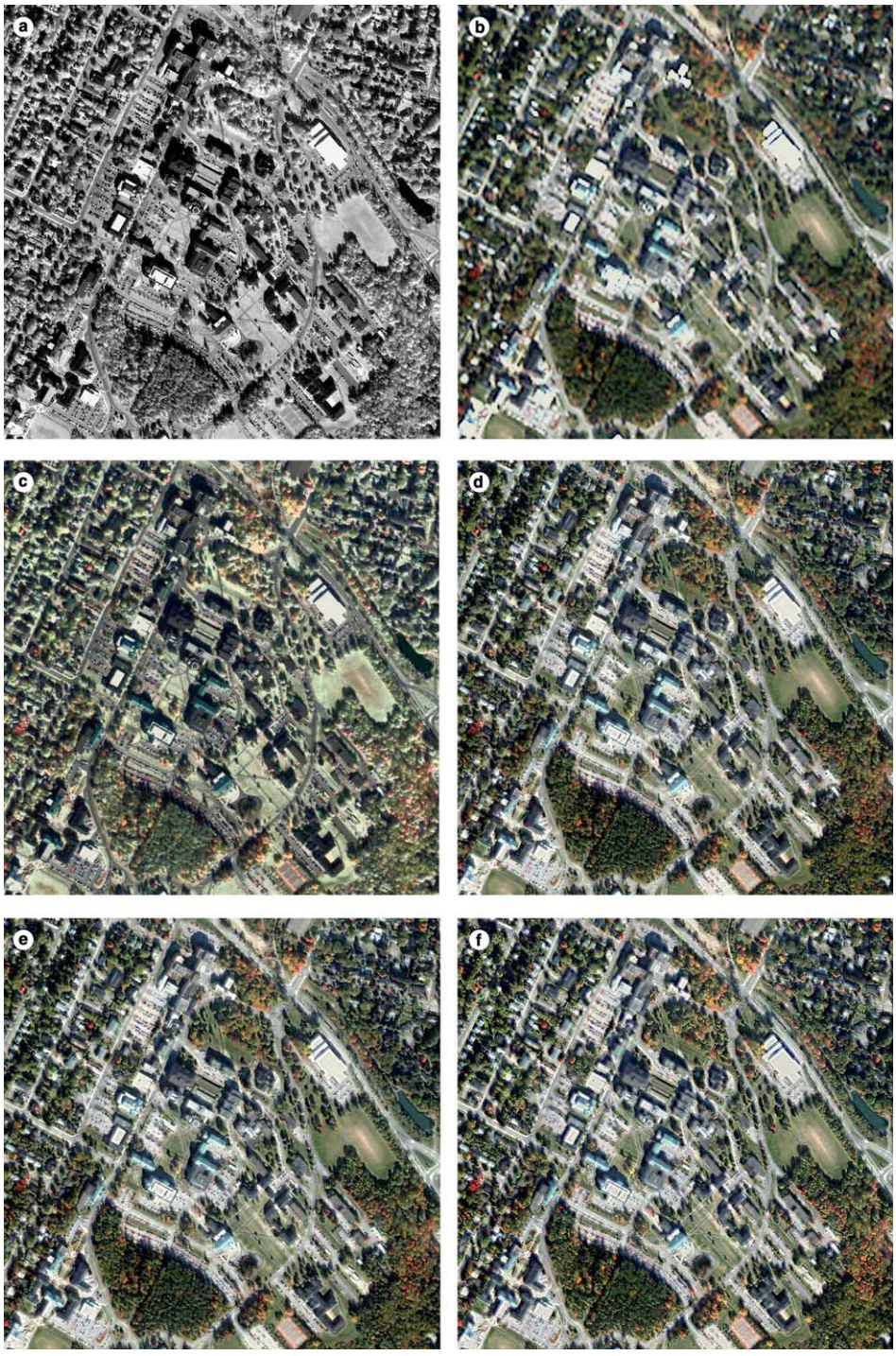

Fig. 3. Fusion results of different algorithms. (a) The source panchromatic image; (b) the source multispectral image (has been resampled to the same size of the 1-m resolution panchromatic image); (c) fused image by the IHS transform based algorithm; (d) fused image by the DWT based algorithm; (e) fused image by the DWFT based algorithm; (f) fused image by the proposed algorithm.

Step 8. Finally, the fused image F is obtained by converting the achromatic and chromaticity channels (l', α_S, β_S) into the RGB color space.

4. Experiment results

The test images are downloaded from http://studio.gge.unb.ca/UNB/zoomview/examples.html. The 1-m resolution panchromatic image and the 4-m resolution multispectral image (shown in color image by mapping three bands of the multispectral image into the RGB color space) of the city of Fredericton, Canada, are shown in Fig. 3(a) and (b), respectively. These images are acquired by a commercial satellite IKONOS, which collects 1-m resolution panchromatic images and 4-m resolution multispectral images. The raw multispectral image downloaded from the web has been resampled to the same size of the panchromatic image in order to perform image registration.

When performing our image fusion algorithm, we select the $(9,7)$-taps biorthogonal filters as the 1-dimensional prototype filters for designing the non-separable filters. The decomposition level of the NWFT is 5. The other fusion algorithms based on the IHS transform, the DWT (Zhou et al., 1998) and the DWFT (Li et al., 2002) are also performed. The $(9,7)$-taps biorthogonal filters are also used for the DWT and the DWFT decomposition with both the decomposition level of 3 as described in (Li et al., 2002). Fused images by different algorithms are shown in Fig. 3(c)–(f).

A good fusion scheme should preserve the spectral characteristics of the source multispectral image as well as the high spatial resolution characteristics of the source panchromatic image. In this paper, two evaluation criteria are used for quantitative assessment of the fusion performance. The spectral quality of a $P \times Q$ fused image can be measured by the discrepancy D_k at each band:

$$D_k = \frac{1}{P \cdot Q} \sum_{x=1}^{P} \sum_{y=1}^{Q} |F_k(x,y) - L_k(x,y)|, \quad k = R, G, B, \tag{26}$$

where $F_k(x,y)$ and $L_k(x,y)$ are the pixel values of the fused and original mutispectral images at position (x,y), respectively, in this paper $P = 879$, $Q = 883$. A small discrepancy implies a good fusion result. For the spatial quality, we use the average gradient to evaluate the performance of the fused image F. That is

$$ag_k = \frac{1}{(P-1)(Q-1)} \times \sum_{x=1}^{P-1} \sum_{y=1}^{Q-1} \sqrt{\frac{\left(\frac{\partial F_k(x,y)}{\partial x}\right)^2 + \left(\frac{\partial F_k(x,y)}{\partial y}\right)^2}{2}}, \quad k = R, G, B, \tag{27}$$

where $F_k(x,y)$ is the pixel value of the fused image at position (x,y). The average gradient reflects the clarity of the fused image. It can be used to measure the spatial resolution of the fused image,

Table 1
Spectral discrepancies between the fused images and the source multispectral image

	R	G	B
The IHS transform based algorithm	46.5065	46.7510	47.2055
The DWT based algorithm	23.4089	23.2558	24.4334
The DWFT based algorithm	22.4450	22.3633	23.4603
The proposed algorithm	20.1051	20.2990	20.7479

Table 2
Average gradients of the fused images

	R	G	B
The IHS transform based algorithm	21.9819	21.9593	21.4993
The DWT based algorithm	19.9665	19.9251	19.6717
The DWFT based algorithm	19.7988	19.7545	19.4871
The proposed algorithm	20.8022	20.7016	20.2594

i.e., a larger average gradient means a higher spatial resolution. Table 1 shows the spectral discrepancies between the images obtained by different fusion algorithms and the source multispectral image. The average gradients of the images obtained by different fusion algorithms are shown in Table 2. From these two tables, we can conclude that the proposed algorithm can preserve high spatial resolution characteristics of the source panchromatic image. In addition, the spectral distortion introduced to the proposed fusion method is less than the traditional algorithms based on the IHS transform, the DWT and the DWFT.

5. Conclusions

A novel color transfer based image fusion algorithm using the NWFT is presented in this paper. There are no papers using color transfer in the $l\alpha\beta$ color space to fuse panchromatic and multispectral images. The axes in the $l\alpha\beta$ color space are decorrealated. This characteristic is more suitable to process color information, because we can apply different operations in different color channels without causing cross-channel artifacts. The NWFT decomposition of an image is performed on areas instead of rows and columns. This transform is also suitable for the multiresolution decomposition of an image, because most 2-dimensional signals cannot be processed separately in x and y directions. Experiment results confirm the effectiveness of the proposed fusion algorithm in fusing real-life remote sensing images.

Acknowledgments

This work was jointly supported by National Natural Science Foundation of China (60375008), China Aviation Science Foundation (02D57003), China Ph.D. Discipline Special Foundation (20020248029), Aerospace Supporting Technology Foundation (2003-1.3 02), EXPO Special Project of National Key Technologies R&D Programme (2004BA908B07), Shanghai Key Technologies Pre-research Project (035115009).

References

Carper, W.J., Lillesand, T.M., Kiefer, R.W., 1990. The use of intensity-hue-saturation transformations for merging SPOT panchromatic and multispectral image data. Photogramm. Eng. Rem. Sens. 56 (4), 459–467.

Chavez, P.S., Kwarteng, A.Y., 1989. Extracting spectral contrast in Landsat thematic mapper image data using selective component analysis. Photogramm. Eng. Rem. Sens. 55 (3), 339–348.

Chavez, P.S., Sildes, S.C., Anderson, J.A., 1991. Comparison of three different methods to merge multiresolution and multispectral data: Landsat TM and SPOT panchromatic. Photogramm. Eng. Rem. Sens. 57 (3), 295–303.

Civco, D.L., Wang, Y., Silander, J.A., 1995. Characterizing forest ecosystems in Connecticut by integrating Landsat TM and SPOT panchromatic data. In: Proceedings 1995 Annual ASPRS/ACSM Convention, Charlotte, NC. 2, pp. 216–224.

Kovačević, J., Vetterli, M., 1992. Nonseparable multidimensional perfect reconstruction filter banks and wavelet bases for R^n. IEEE Trans. Inform. Theory 38 (2), 533–555.

Kovačević, J., Vetterli, M., 1995. Nonseparable two- and three-dimensional wavelets. IEEE Trans. Signal Process. 43 (5), 1269–1273.

Li, H., Manjunath, B.S., Mitra, S.K., 1995. Multisensor image fusion using the wavelet transform. Graph. Model. Image Process. 57 (3), 235–245.

Li, S., Kwok, J.T., Wang, Y., 2002. Using the discrete wavelet frame transform to merge Landsat TM and SPOT panchromatic images. Inform. Fusion 3 (1), 17–23.

Pan, J.S., Wang, J.W., 1999. Texture segmentation using separable and non-separable wavelet frames. IEICE Trans. Fundam. E82-A (8), 1463–1474.

Reinhard, E., Ashikhmin, M., Gooch, B., Shirley, P., 2001. Color transfer between images. IEEE Computer Graph. Appl. 21 (5), 34–41.

Ruderman, D.L., Cronin, T.W., Chiao, C.C., 1998. Statistics of cone responses to natural images: Implications for visual coding. J. Opt. Soc. Amer. A 15 (8), 2036–2045.

Shettigara, V.K., 1992. A generalized component substitution technique for spatial enhancement of multispectral images using a higher resolution data set. Photogramm. Eng. Rem. Sens. 58 (5), 561–567.

Welsh, T., Ashikhmin, M., Mueller, K., 2002. Transferring color to greyscale images. ACM Trans. Graph. (TOG) 21 (3), 277–280.

Yockey, D.A., 1995. Image merging and data fusion by means of the discrete two-dimensional wavelet transform. J. Opt. Soc. Amer. A 12 (9), 1834–1841.

Zhou, J., Civco, D.L., Silander, J.A., 1998. A wavelet transform method to merge Landsat TM and SPOT panchromatic data. Internat. J. Rem. Sens. 19 (4), 743–757.